Control of Aeroelastic Divergence

Richard R. Chipman,* Alex M. Zislin,† and Catherine Waters‡
Grumman Aerospace Corporation, Bethpage, New York

On forward-swept-wing aircraft, aerodynamic destiffening of the primary wing-bending mode can cause coupling with the short-period mode, potentially resulting in a low-frequency dynamic instability. For a clamped wing this coupled mechanism degenerates into conventional static wing divergence. Studies of a fundamental analytical model of this mechanism show that active control of the clamped wing is possible only through the use of displacement feedback. Control laws for the clamped wing are evaluated and also assessed when body freedom is restored. Additionally, control laws are synthesized directly for a more refined representation of the unrestrained vehicle. Control configured vehicles (CCVs) are not considered.

Nomenclature

A, A_1, etc. = state matrices [Eqs. (8) and (9)]
b = reference semichord
b_l = damping defined in Eq. (24)
B, B_1, etc = control matrices [Eqs. (8) and (9)]
c = stiffness defined in Eq. (24)
d = gain
D = feedback gains
D^{opt} = optimal feedback gains
E = measurement matrix [Eq. (12)]
f = feedback
G, G_1 = gust matrices [Eqs. (8) and (9)]
h = physical displacements
J = performance index
K = generalized stiffness matrix
L = number of aerodynamic lag states
L_0 = turbulence scale
M = generalized mass matrix
NC = number of controls
P = solution to matrix Ricatti equation
p_l = pole locations for aerodynamic lag states
q = dynamic pressure
q_o^* = dynamic pressure at the open-loop design point
q_c^* = dynamic pressure at the closed-loop divergence point
Q = generalized aerodynamic force
$\tilde{Q}$ = state quadratic weighting
R = feedback quadratic weighting
s = Laplace variable
$\bar{s}$ = scaled Laplace variable, $= bs/V$
t = time
u = actuator input (feedback)
v = control states
V = airplane velocity
W_g = gust velocity
$W_{g,l}$ = gust aerodynamic lag states
x = aircraft or plant states
y = measurements
z = gust states
δ = control surface deflections
δ_l = control aerodynamic lag states
ζ_a = actuator damping ratio
η = white noise forcing function
λ = eigenvalue
ξ = generalized coordinates
ξ_l = generalized coordinate aerodynamic lag states
σ = rms gust velocity
Φ = normal modes
ω_a = actuator frequency

Presented as Paper 82-0684 at the AIAA/ASME/ASCE/AHS 23rd Structures, Structural Dynamics and Materials Conference, New Orleans, La., May 10-12, 1982; submitted May 28, 1982; revision received June 7, 1983.

*Engineering Specialist, Aeroelasticity. Member AIAA.
†Senior Engineer, Guidance and Control. Member AIAA.
‡Group Leader, Loads and Dynamics.

Introduction

To avoid aeroelastic divergence, forward-swept-wing (FSW) designs tend to be stiffness rather than strength critical. In fact, the weight penalty imposed on metallic forward-swept wings to obtain the necessary stiffness level has been substantial enough to virtually preclude such designs. Through the use of proper fiber layups, however, recent studies[1] demonstrate the required stiffness can be obtained in composite structures with little or no weight penalty relative to the strength design. This successful structural design solution to wing divergence might be thought to obviate the need for research into the use of active control technology for divergence suppression. However, such a conclusion is premature, since expanded missions (i.e., additional store carriage requirements) that might evolve for a FSW aircraft after the structural design is frozen could cause divergence to reappear within the flight envelope. Thus, the exploration of active-control concepts for divergence suppression is potentially as profitable as similar studies[2-7] that have been made of flutter suppression.

This paper addresses the use of active controls for divergence suppression and focuses on a simple analytical model of the phenomenon that retains its fundamental characteristics. Such a model is employed to obtain a clear understanding of the basic mechanisms involved in the uncontrolled (open-loop) and controlled (closed-loop) systems. Control laws are synthesized both by semi-intuitive means and through the use of linear optimal control techniques. Emphasis is placed on the physical interpretation of the designs.

Theory

General Formulation

Using undamped natural vibration modes, the deformation of a flexible aircraft can be expressed as

$$h = \Phi \cdot \xi(t) \tag{1}$$

where rigid-body modes can be included if necessary. The equations of motion then can be written in generalized coordinates as

$$M\ddot{\xi} + K\xi = q(Q^{\xi}\xi + Q^{\delta}\delta + Q^{g}W_g) \tag{2}$$

In linear speed regimes, generalized aerodynamic forces can be computed for harmonic motion at selected frequencies by using various unsteady lifting surface theory codes, such as the doublet-lattice method[8] for subsonic flow and the Mach box method[9] for supersonic flow. Using the Pade fitting technique[3] each of the aerodynamics matrices can be approximated in the Laplace domain by series of the form.

$$Q(s) = Q_0 + \bar{s}Q_1 + \bar{s}^2 Q_2 + \sum_{\ell=3}^{L} \frac{\bar{s}}{\bar{s}+p_\ell} Q_\ell \tag{3}$$

(Usually, the terms Q_1^g and Q_2^g can be omitted.) Using this representation and identifying powers of s as time derivatives, Eq. (2) can be recast as

$$M\ddot{\xi} + K\xi = q\left(Q_0^\xi \xi + \frac{b}{V} Q_1^\xi \cdot \dot{\xi} + \left(\frac{b}{V}\right)^2 Q_2^\xi \cdot \ddot{\xi} + \sum_{l=3}^{L} Q_l^\xi \cdot \xi_l\right) + q\left(Q_0^\delta \cdot \delta + \frac{b}{V} Q_1^\delta \cdot \dot{\delta} + \left(\frac{b}{V}\right)^2 Q_2^\delta \cdot \ddot{\delta} + \sum_{l=3}^{L} Q_l^\delta \cdot \delta_l\right) + q\left(Q_0^g \cdot W_g + \sum_{l=3}^{L} Q_l^g \cdot W_{g,l}\right) \tag{4}$$

where, for example, the aerodynamic lag states for the generalized coordinates are related to these coordinates by

$$\dot{\xi}_l + \frac{V}{b} p_l \cdot \xi_l = \dot{\xi} \tag{5}$$

Next, models of the control-surface actuator dynamics and the gust spectrum can be introduced. For example, the transfer functions for a second-order actuator and for converting white noise to the Dryden gust spectrum[10] are, respectively,

$$\frac{\delta_i}{u_i} = \frac{\omega_{a_i}^2}{s^2 + 2\zeta_{a_i}\omega_{a_i} s + \omega_{a_i}^2}, \qquad i = 1,\ldots,NC \tag{6}$$

and

$$\frac{W_g}{\eta} = \sigma\sqrt{\frac{3V}{L_0}} \frac{s + V/L_0\sqrt{3}}{(s+V/L_0)^2} \tag{7}$$

Combining Eqs. (4-7) the following state variable formulation can be obtained:

$$\begin{bmatrix} \dot{x} \\ \dot{v} \\ \dot{z} \end{bmatrix} = \begin{bmatrix} A_1 & A_2 & A_3 \\ 0 & A_4 & 0 \\ 0 & 0 & A_5 \end{bmatrix} \cdot \begin{bmatrix} x \\ v \\ z \end{bmatrix} + \begin{bmatrix} B_1 \\ B_2 \\ 0 \end{bmatrix} \cdot u + \begin{bmatrix} 0 \\ 0 \\ G_1 \end{bmatrix} \cdot \eta \tag{8}$$

or

$$\dot{X} = A \cdot X + B \cdot u + G \cdot \eta \tag{9}$$

where the plant, control, and gust vectors (x,v,z) are comprised of their respective states, rates, and lags. Details of this manipulation are given in Refs. 2 and 7.

Stability of the open-loop system can be determined by computing the eigenvalues of the real-coefficient linear system

$$\dot{X} = A \cdot X \tag{10}$$

To exercise control of the system, feedback of a set of measurements, which are linear functions of the states, is introduced:

$$u = D \cdot y \tag{11}$$

$$y = E \cdot x \tag{12}$$

Thus, the equations of the closed-loop system are

$$\dot{X}(A + BDE) \cdot X + G \cdot \eta \tag{13}$$

and stability can be determined from the eigenvalues of

$$\dot{X} = (A + BDE) \cdot X \tag{14}$$

Optimal Control Theory Overview

The realization of the equations of motion with unsteady aerodynamics in state variable form allows the power of linear optimal control theory to be directly applied to the problem of suppression of aeroelastic instabilities. Specifically, for a physical system described by

$$\dot{X} = A \cdot X + B \cdot u \tag{15}$$

An optimal set of feedback gains can be obtained such that

$$u = D^{\text{opt}} X \tag{16}$$

The optimization problem can be stated simply as: Given a quadratic performance index of the form

$$J = \int_{t_0}^{t_f} (x^T \hat{Q} x + u^T R u)\, dt \tag{17}$$

find the control u which minimizes J subject to the constraint of Eq. (15).

The solution for the optimal gains D^{opt} can be obtained by using dynamic programming or the maximum principle. This leads to

$$D^{\text{opt}} = -R^{-1} B^T P \tag{18}$$

where P is the solution of the matrix Ricatti equation

$$\dot{P} = PA + A^T P - PBR^{-1} B^T P + \hat{Q} \tag{19}$$

Since the most useful solution is that which gives a time-invariant gain matrix, we have found the best approach is to use Potter's technique to obtain the steady-state P matrix.[11,12]

Fundamental Static-Divergence Model

Using the doublet-lattice program,[8] harmonic generalized aerodynamic forces were generated at Mach 0.90, sea level, for a forward-swept wing planform with the aerodynamic paneling shown in Fig. 1. Thirteen free-free symmetric modes—rigid-body heave and pitch, the first ten flexible modes, and an outboard flap-rotation mode—obtained from a realistic composite FSW design were modeled. Additionally, forces for a harmonic gust were computed.

Standard k-method analyses[13] of the system were performed which revealed that the instability speed could be computed to within 1% accuracy while omitting all but the rigid and first three flexible modes. Pade representations of the form of Eq. (3) (with four lag terms) were then obtained

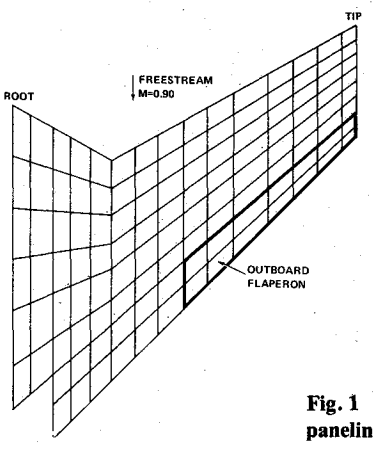

Fig. 1 Doublet-lattice aerodynamic paneling for FSW.

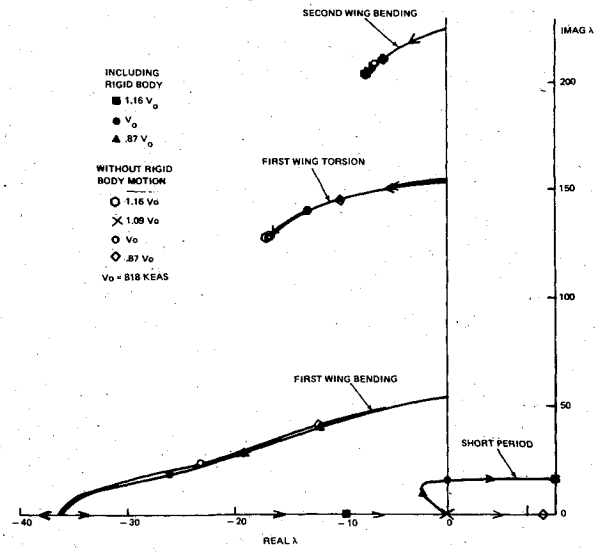

Fig. 2 Open-loop velocity root loci for FSW.

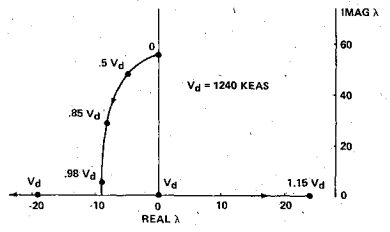

Fig. 3 Open-loop velocity root locus, fundamental model problem.

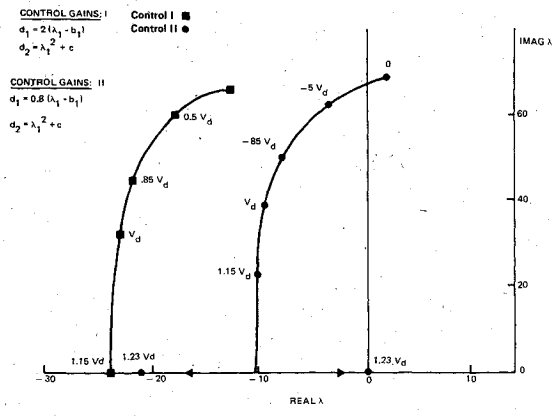

Fig. 4 Closed-loop velocity root locus, controls I and II.

for the generalized aerodynamic forces, and eigenvalues of Eq. (10) were computed for various airspeeds. The resulting velocity root loci are shown in Fig. 2. The predicted instability speed is within 0.05% of that obtained by the k method. The basic mechanism is a low-frequency dynamic instability caused by the coupling of the short-period rigid-body mode with the wing first bending mode which rapidly destiffens within increasing airspeed. These characteristics agree with those of Ref. 14. Additional analyses were performed omitting the rigid-body modes. As also shown in Fig. 2, the wing first bending mode continues to destiffen and diverges statically at a slightly (9%) higher airspeed. This illustrates that the essential ingredient in the instability of realistic FSW configurations is the destiffening of the wing bending mode; the frequency of the true dynamic instability is so low that reasonably accurate predictions are obtained treating the problem as if it were purely static divergence. Furthermore, as shown in Fig. 3, this static wing divergence can be predicted qualitatively using a single flexible mode—wing first bending. Consequently, to obtain a fundamental understanding of the occurrence and control of the aeroelastic instability of forward-swept wings, the simple one-mode representation was adopted as an initial model problem. After study of this model problem, investigation of the comprehensive representation was undertaken.

For the elementary model, Eq. (2) is simplified to a scalar equation.

$$M_1\ddot{\xi}+K_1\xi=q(\bar{Q}\xi+\bar{Q}_\delta\delta+\bar{Q}_g W_g) \tag{20}$$

Since we are interested in a static instability, a low-frequency approximation to Eq. (3) is acceptable.

$$Q(s)=Q_0+\bar{s}Q_1 \tag{21}$$

Thus, Eq. (4) becomes

$$M_1\ddot{\xi}+K_1\xi=q(\bar{Q}_0\xi+\frac{V}{b}\bar{Q}_1\dot{\xi})+q\left(\bar{Q}_{0,\delta}\delta+\frac{V}{b}Q_{1,\delta}\dot{\delta}\right)$$

$$+q\bar{Q}_{0,g}W_g \tag{22}$$

and the stability of the open-loop system is determined from the characteristic values of

$$M_1\ddot{\xi}-q\left(\frac{V}{b}\bar{Q}_1\dot{\xi}\right)+\left(K_1-q\bar{Q}_0\right)\xi=0 \tag{23}$$

that is,

$$\lambda=-b_1\pm\sqrt{b_1^2+c}$$

$$b_1=\frac{q}{2}\left(\frac{V}{b}\right)\bar{Q}_1/M_1, c=(q\bar{Q}_0-K_1)/M_1 \tag{24}$$

Static instability is seen to occur when $qQ_0>K_1$, i.e., when the aerodynamic destiffening exceeds the structural stiffness.

Divergence Suppression for the Elementary Model

Including a feedback force, Eq. (23) can be rewritten as

$$\ddot{\xi}+2b_1\dot{\xi}-c\xi+df=0 \tag{25}$$

Examination of this simple equation clarifies the issue (raised in Ref. 15) of what type of feedback is required to suppress divergence: For static divergence of the open-loop system to occur, b_1 and c must be positive. If acceleration feedback ($f=\ddot{\xi}$) is attempted, the eigenvalues of the closed-loop system are

$$\lambda=\frac{-b_1}{1+d}\pm\sqrt{\left(\frac{b_1}{1+d}\right)^2+\frac{c}{1+d}} \tag{26}$$

Thus, the system cannot be stabilized by any choice of gain; variations of the gain produce either a static or dynamic instability. If rate feedback ($f=\dot{\xi}$) is attempted,

$$\lambda=-\left(b_1+\frac{d}{2}\right)\pm\sqrt{\left(b_1+\frac{d}{2}\right)^2+c} \tag{27}$$

and a static instability results regardless of the value of the gain chosen. Finally, if displacement feedback ($f=\xi$) is used,

$$\lambda=-b_1\pm\sqrt{b_1^2+(c-d)} \tag{28}$$

and stable solution is possible when the gain exceeds c. Hence only the feedback of displacement can stabilize static divergence. These findings are in agreement with the results of Ref. 15, in which divergence suppression was attempted using each of the three types of feedback.

It is noted that, although displacement feedback is required for divergence suppression, the direct measurement of this state (flexible deformation) is not necessarily required. Since displacement measurements are difficult to accomplish on an aircraft in flight, while accelerometer measurements are routine, appropriate shaping filters can be used in the feedback path to produce displacements from measurements of acceleration. Furthermore, since the desired feedback quantity is generalized (modal) displacement rather than physical displacement, the shaping filter network is more properly thought of as an estimator or an observer network. (From a limited number of physical measurements, the observer network constructs estimates of the desired system states such as wing-bending generalized displacement. The theory and use of such networks is well developed so that its application to this problem is practical.) Consequently, to assure proper sensor placement, accompanying observability studies should be made.

Although, as previously stated, the rate feedback by itself cannot stabilize a statically unstable system, it can be useful in obtaining desirable subcritical characteristics at off-design conditions. To investigate this point, divergence suppression control laws that use a blend of displacement and rate feedback were formulated for the model problem. The

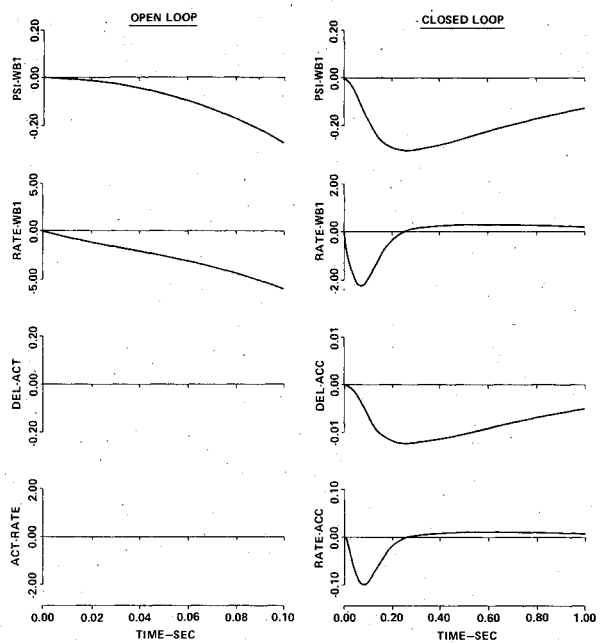

Fig. 5 Open- and closed-loop (control IVA) responses due to 1.0 ft/s gust at $V = 1.15V_d$.

Table 1 Eigenvalues at design point (1.15 V_d) Model problem, no lags: control III.

No.	Open Loop Real	Open Loop Imaginary	Closed loop Real	Closed loop Imaginary
1	18.3	0.0	−18.3	0.0
2	−47.9	0.0	−47.9	0.0
3	−19.1	19.1	−19.1	19.1
4	−19.1	−19.1	−19.1	−19.1
5	−37.8	289.7	−37.9	289.7
6	−37.8	−289.7	−37.8	−289.7

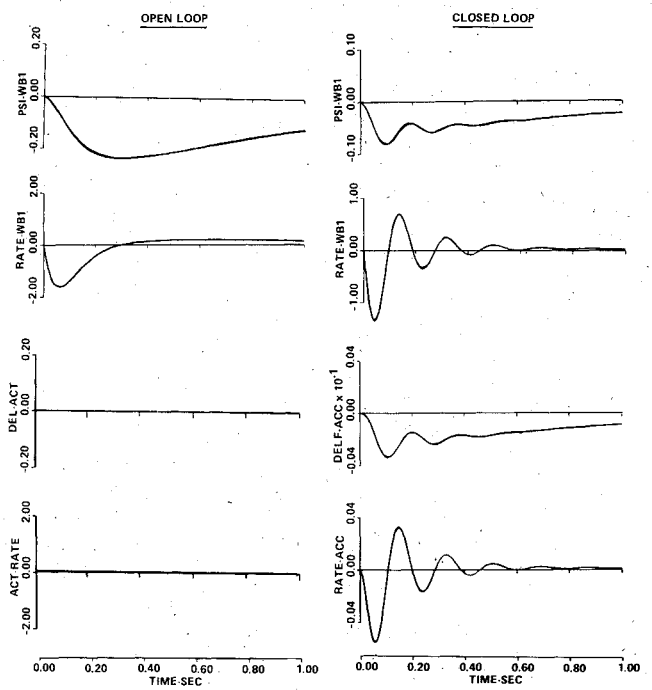

Fig. 6 Open- and closed-loop (control IVA) responses due to 1.0 ft/s gust at $V = 0.96V_d$.

Table 2 Eigenvalues at design point ($V = 1.5V_d$). Model problem, (4 lags): control laws IV and IVA.

No.	Open loop Real	Open loop Imaginary	Closed loop IV Real	Closed loop IV Imaginary	Closed loop IVA Real	Closed loop IVA Imaginary
1	16.8	0.0	−16.8	0.0	−13.1	0.0
2	−46.5	0.0	−46.5	0.0	−46.6	0.0
3	−46.5	0.0	−46.5	0.0	−46.6	0.0
4	−93.0	0.0	−93.0	0.0	−93.0	0.0
5	−93.0	0.0	−93.0	0.0	−93.2	0.0
6	−110.4	0.0	−110.4	0.0	−117.5	9.3
7	−124.7	0.0	−124.7	0.0	−117.5	−9.3
8	−185.6	0.0	−185.6	0.0	−185.7	0.0
9	−186.0	0.0	−186.0	0.0	−186.3	0.0
10	−553.7	0.0	−553.7	0.0	−554.1	0.0
11	−558.1	0.0	−558.1	0.0	−559.0	0.0
12	−597.2	0.0	−597.2	0.0	−597.6	0.0
13	−50.1	5.3	−50.1	5.3	−53.1	6.8
14	−50.1	−5.3	−50.1	−5.3	−53.1	−6.8
15	−19.1	19.1	−19.1	19.1	−18.3	22.1
16	−19.1	−19.1	−19.1	−19.1	−18.3	−22.1
17	−22.7	280.6	−22.7	280.6	−22.6	280.6
18	−22.7	−280.6	−22.7	−280.6	−22.6	−280.6

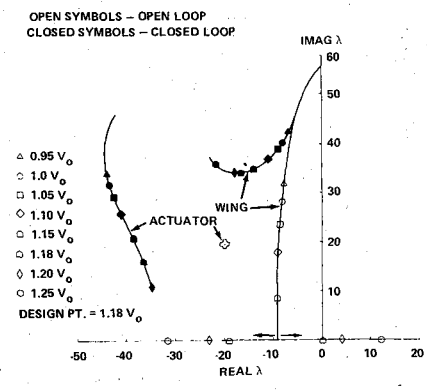

Fig. 7 Root loci for fundamental problem, control V (clamped-wing design).

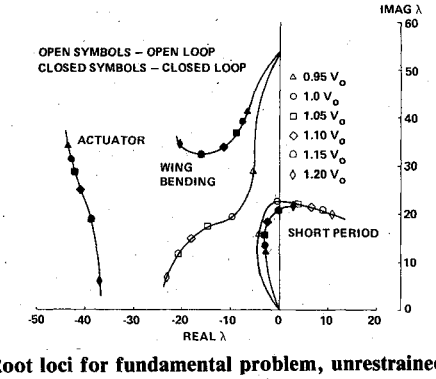

Fig. 8 Root loci for fundamental problem, unrestrained, control V (clamped-wing design).

equation of motion for this system becomes

$$\ddot{\xi}+(2b_1+d_1)\dot{\xi}-(c-d_2)\xi=0 \tag{29}$$

If the open-loop system's unstable root is denoted λ_1, the following choice of gains d_1 and d_2 reflects this root about the imaginary axis to produce a critically damped system:

$$d_1=2(\lambda_1-b_1) \quad \text{and} \quad d_2=\lambda_1^2+c \tag{30}$$

In this case, the closed-loop system is stable at the design point and statically unstable at a higher dynamic pressure given by

$$q_c^*=q_o^*+\frac{M_1}{\bar{Q}_0}\lambda_1^2 \tag{31}$$

Choosing a design point 15% above the divergence speed, gains were computed using this approach. Figure 4 depicts the root loci for this design (control law I). Notice that the control changes the zero-airspeed characteristics of the system. This is a significant fact to keep in mind as illustrated also in this figure by control law II. Here a gain d_1 equal to 40% of its previous value still stabilizes the system at the design point but causes it to be unstable at zero airspeed. Thus, in a general case, gain scheduling might be necessary to keep the system stable throughout the speed regime.

Optimal Control Theory Applied to a Fundamental Model

Optimal control theory was applied to the fundamental model first. A flap-rotation mode and a second-order actuator [Eq. (6)] were included in the analysis. The design objective was a 15% increase in the clamped-wing divergence speed and, hence, in the limit operating point speed, with moderate control requirements (i.e., actuator deflection and rate) at the operating point. The design point was set at 15%

Table 3 rms responses due to 1.0 ft/s rms gust at a speed near the new operating point ($V=0.96\ V_d$) using control law IVA

	rms state responses			
	Wing first bending[a]		Actuator	
	Displacement[a]	Rate[a]	Displacement, deg	Rate, deg/s
Open loop	0.23	1.15	0.0	0.0
Closed loop	0.06	0.83	0.14	2.05

[a]Units are in normalized modal coordinates; a displacement of 30.0 would correspond to a limit-load wing-root bending moment.

in velocity above the new limit operating point, the latter being equal to the open-loop clamped-wing divergence speed. The control requirements were judged by computing at these speeds the closed-loop response due to random turbulence characterized by Eq. (7). In particular, rms values of various system states (e.g., wing first bending displacement and rate, and actuator displacement and rate) due to 1 ft/s rms gust, and time histories of the responses to an instantaneously applied 1 ft/s gust were examined. The maximum allowable rms values of actuator displacement and rate at the new limit operating point were taken to be 0.4 deg and 4.0 deg/s for the 1 ft/s rms gust (or, equivalently, 10 deg and 100 deg/s for a peak of three times the response to an 8.3 ft/s rms gust). Since the design point is outside the expanded operating envelope, no maximum allowable responses were set at this point; these responses were examined only to compare control laws.

Initially, optimal full-state feedback gains were obtained using zero state weighting [$\hat{Q}=0$ in Eq. (17)]. This weighting causes the open-loop unstable root to be reflected about the imaginary axis in the closed-loop condition (see Table 1). Thus this design (control law III) is similar to control law I discussed above; it differs from control law I because of the inclusion of flap and actuator dynamics.

Before examining responses, zero state weighting gains (control law IV) were obtained for a more realistic model including aerodynamic lag states. Since this control law includes gains on the lag states, a more practical control (control law IVA) was formed by simply zeroing out these lag-state gains. Table 2 presents the design point eigenvalues for these designs. As can be judged by examining the first eigenvalue, control IVA is slightly less stable than control IV.

In Table 3 the open- and closed-loop (control IVA) rms responses are shown at a point slightly below the limit operating point. (At the exact limit operating point the open-loop system is unstable.) Actuator responses are well within their maximum allowable limits. Notice also that the control significantly reduces the wing-bending responses; thus, the control may be useful as a gust load alleviation system as well as a divergence suppression system.

Figures 5 and 6 show the open- and closed-loop responses at the design and operating points, respectively, to an instantaneous 1 ft/s gust. (Note that both the horizontal and vertical scales differ between the open- and closed-loop plots.) As can be inferred from Fig. 5, the closed-loop system is critically damped in its dominant mode at the design point. Figure 6 shows that near the operating point the closed-loop system has a damped oscillatory behavior. Again, it can be seen that the closed-loop wing responses are less than their open-loop counterparts.

Initial Synthesis of Control Laws for an Unrestrained Vehicle

Because the essential ingredient in the aeroelastic instability of FSW configurations is the destiffening of the wing first bending mode, the obvious approach is to develop control laws using the clamped-wing system and try to apply them to the unrestrained vehicle. This is demonstrated in the following paragraphs; first for the one-wing-mode idealization and then for the more comprehensive three-wing-mode model.

Fundamental Model

Control laws were synthesized using the fundamental one-wing-mode model. The design point was chosen to be 18% above the airspeed at which instability occurs in the idealization comprised of the combination of this one-wing mode and the two rigid-body modes. In the performance index [Eq. (17)], a nonzero state weighting factor was put only on the wing mode generalized coordinate. The weight chosen was one hundredth of the weight on the control; i.e., $Q=0.01R$. Figure 7 shows the open- and closed-loop velocity root loci for the fundamental problem. As can be seen, stability is obtained by retarding the destiffening of the wing mode. This control law is denoted V.

The control law derived for the fundamental model (i.e., feedback gains on ξ, $\dot{\xi}$, δ, $\dot{\delta}$ and δ) was then evaluated for the system with the rigid-body modes included. Figure 8 presents the open- and closed-loop velocity root loci for this system. As can be seen, the control law stabilizes the system up to 15% above the airspeed at which open-loop instability occurs. Thus, for this case the clamped-wing-derived control laws stabilize the unrestrained system almost up to the target speed. That the increase in stability produced by this synthesis procedure is somewhat less (3% in airspeed) than desired should not be surprising. The loss in stability margin is due to the effect of unmodeled system states (i.e., rigid-body motions). Also the damping levels in the short-period mode at subcritical speeds are less than would be desirable in an aircraft final design.

Three-Wing-Mode Model

The same procedure was used for the more comprehensive three-wing-mode model, producing control law VI. Here the design point was chosen to be $1.12V$ and state weighting was placed on the first wing mode ($0.01R$) and its rate ($0.001R$). Figures 9 and 10 show the root loci for the restrained and unrestrained vehicles, respectively. Once again the restrained vehicle control laws are seen to increase (by 9% in airspeed) the stability of the unrestrained system.

The two demonstrations suggest that this procedure can achieve moderate (say, 10%) increases in the stability speed limit without much effort. However, for larger increases it may be more straight forward to include the rigid-body motions directly in the synthesis.

Table 4 rms responses to 1.0 ft/s rms gust at a speed near new operating point ($V=0.99\ V_0$) using control law VII

	rms responses			
	Wing tip motion		Actuator motion	
	Flexible displacement, ft	Total Acceleration, g	Deflection, deg	Rate, deg/s
Open loop	0.088	0.51	0.0	0.0
Closed loop	0.011	0.47	0.24	5.2

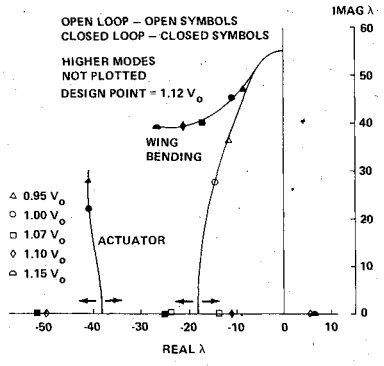

Fig. 9 Root loci for restrained vehicle, control VI (clamped-wing design).

Direct Synthesis for an Unrestrained Vehicle

For a more comprehensive control design, the synthesis procedure was applied directly to the model of the unrestrained vehicle. Rigid-body modes, the three lowest

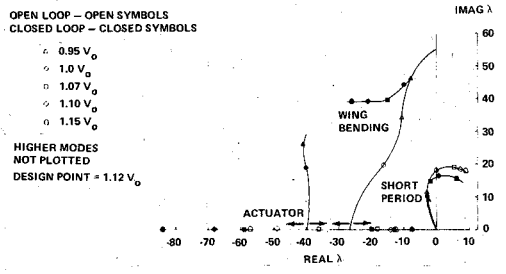

Fig. 10 Root loci for unrestrained vehicle, control VI (clamped-wing design).

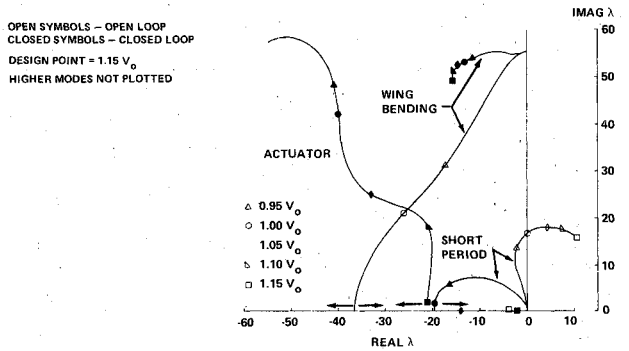

Fig. 11 Root loci for unrestrained vehicle, control VII (unrestrained vehicle design).

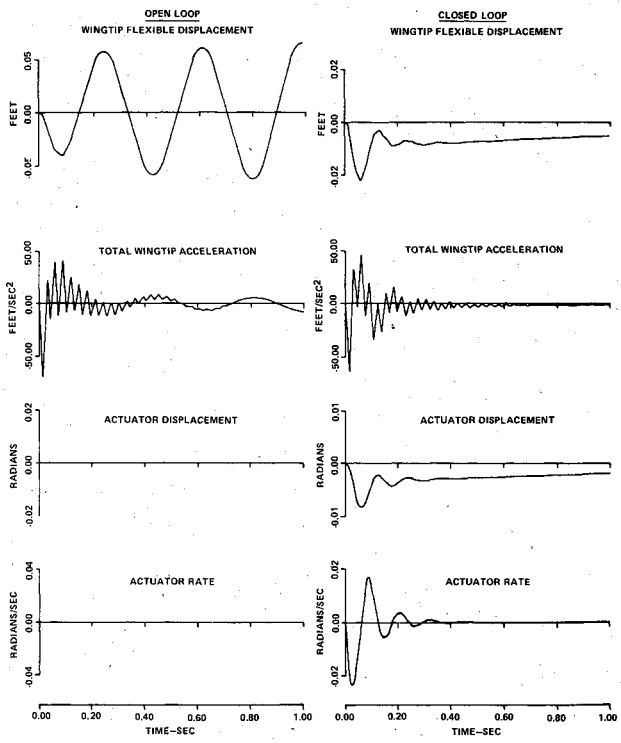

Fig. 12 Open- and closed-loop (control VII) responses at $0.99V_0$ due to 1.0 ft/s gust.

flexible-wing modes, the actuator, and corresponding aerodynamic lag states (four per mode) were included. The design point was chosen at $1.15V_0$ (15% above the open-loop unrestrained vehicle instability). First, a zero state weighting design was attempted; but the results were unacceptable at subcritical speeds. Building on the experience gained from the clamped-wing studies, the next designs were done with state weighting on the first wing bending mode and its rate. Some variations in the ratio of these weights to the control weight were made; the final design was done with a ratio of $\hat{Q}_\xi/R = \hat{Q}_{\dot{\xi}}/R = 0.01$. The gains obtained on the aerodynamic lag states were zeroed out (to produce control law VII), and closed-loop root loci were generated. Figure 11 presents both the open- and closed-loop root loci. As can be seen, stability has been increased by more than 15% in airspeed.

Response of four selected physical parameters (the flexible deflection and total acceleration of a point near the wing tip, and actuator displacement, and rate) were determined in a statistical and time history sense. For the former, the forcing function spectrum was a 1 ft/s rms Dryden gust. For the latter, a 1 ft/s gust was instantaneously applied. Figure 12 and Table 4 present the responses at the new operating point ($0.99V_0$). Wing deflection has been markedly reduced with a slight decrease in acceleration. Actuator displacement is within acceptable limits, but its rate is somewhat high. Our expectation is that the actuator rate can be reduced through a few more iterations of the synthesis with variations in the weights.

Conclusions

The essential ingredient in the aeroelastic instability of FSW aircraft is the aerodynamic destiffening of the primary wing-bending mode. On the unrestrained vehicle, this mode couples with the aircraft short-period mode, potentially resulting in a low-frequency dynamic instability within the speed envelope. For a clamped wing this mechanism degenerates into conventional static wing divergence. Active control to prevent or delay the onset of the static instability requires the use of displacement feedback. Active control of the dynamic instability is best achieved by a combination of feedbacks dominated by displacement feedback. In fact, for moderate increases in stability, displacement feedback is sufficient. Thus, control laws synthesized from clamped-wing considerations alone are possible, although this is not always the most straight forward approach. As a consequence, direct syntheses including rigid-body motions were undertaken, using essentially full-state feedback. Reasonable control laws were found for the representative vehicle. Typically, 15% increases in stability speed limit were easily obtained.

Important aspects of active aeroelastic control concepts remain to be addressed; e.g., the use and proper placement of physical sensors to implement the control laws (observer networks and reduced-state feedback), the impact of relaxed static stability typical of tactical FSW aircraft, and the effect of aerodynamic nonlinearities of the transonic regime in which these aircraft will operate.

References

[1] Spacht, G., Calandra, J., et al., "Forward Swept Wing Demonstrator Technology Integration and Evaluation Study," AFWAL-TR-80-3145, Vol. III, Dec. 1980.

[2] Newsom, J., "Control Law Synthesis for Active Flutter Suppression Using Optimal Control Theory," *Journal of Guidance and Control,* Vol. 2, Sept.-Oct. 1979.

[3] Sevart, F., "Development of Active Flutter-Suppression Wind-Tunnel Testing Technology," AFFDL-TR-74-126, 1975.

[4] Abel, I., Perry, B., and Murrow, H., "Two Synthesis Techniques Applied to Flutter Suppression on a Flight Research Wing," *Journal of Guidance and Control,* Vol. 1, Sept.-Oct. 1978.

[5] Noll, T., Huttsell, L., and Cooley, D., "Investigation of International Control Laws for Wing/Store Flutter Suppression," *Proceedings of 21st SDM Conference,* May 1980.

[6] Edwards, J., "Flight Test Results of an Active Flutter Suppression System Installed on a Remotely Piloted Research Vehicle," *Proceedings of AIAA Dynamic Specialist Conference,* April 1981.

[7] Newsom, J. and Pototzky, A., "Comparison of Analysis and Flight Test Data for a Drone Aircraft with Active Flutter Suppression," *Proceedings of AIAA Dynamic Specialist Conference,* April 1981.

[8] Giesing, J., Kalman, T., and Rodden, W., "Subsonic Unsteady Aerodynamics for General Configurations," AFFDL-TR-71-5, Pt. I, Feb. 1971.

[9] Zartarian, G. and Hsu, P., "Theoretical Studies on the Prediction of Unsteady Supersonic Airloads of Elastic Wings," Pts. 1 and 2, WADC-TR-56-97, Feb. 1956.

[10] Liepmann, H., "On the Application of Statistical Concepts to the Buffeting Problem," *Journal of Aerospace Sciences,* Vol. 19, Dec. 1952.

[11] Anderson, B. and Moore, J., *Linear Optimal Control,* Prentice Hall, 1971.

[12] Potter, J., "Matrix Quadratic Solution," *SIAM Journal of Applied Mathematics,* Vol. 14, May 1966.

[13] Bisplinghoff, R. and Ashley, H., *Principles of Aeroelasticity,* Dover Publications, 1975, pp. 379-388.

[14] Weisshaar, T., "Final Report—Divergence Suppression for Forward Swept Wings," NASI-15080-Task 16, VPI&SU, Blacksburg, Va., Sept. 1980.

[15] Griffin, K. and Eastep, F., "Active Control of Forward Swept Wings with Divergence and Flutter Aeroelastic Instabilities," *Proceedings of AIAA Dynamic Specialists Conference,* April 1981.